Tactile Sensing and Terrain-Based Gait Control for Small Legged Robots

X. Alice Wu*, Tae Myung Huh*, Aaron Sabin, Srinivasan A. Suresh, and Mark R. Cutkosky

***Abstract*—For small legged robots, ground contact interactions significantly affect the dynamics and locomotion performance. We designed thin, robust capacitive tactile sensors and applied them to the feet of a small hexapod with C-shaped rotating legs. The sensors measure contact forces as the robot traverses different types of terrain including hard surfaces with high or low friction, sand and grass. Different gaits perform best on different types of terrain. Useful measured parameters include the magnitude and timing of the peak normal forces, in combination with the leg rotational velocity. The measured parameters were used in a SVM classifier to identify terrain types with 82.5% accuracy. Based on gait performance studies, we implemented a terrain-based gait control using real-time terrain classifications. A surface transitioning test shows 17.1% increase in body speed and 13.2% improvement in efficiency as the robot adjusts its gait.**

***Index Terms*—Force and Tactile Sensing, Legged Robots, Sensor-based Control, Terrain Classification, Adaptive Gait Control**

I. Introduction

FOR small legged robots and animals, the details of interactions between their feet and the ground can have a profound effect on the speed and efficiency of locomotion. For example, on grassy terrain, the interactions may dissipate significant energy due to the deformation of the surface. Conversely on hard and smooth surfaces, slippage may be significant. Perhaps of most interest are leg and ground interactions on granular media such as sand and loose soil, which can have a considerable effect on limb kinematics and locomotion performance [1], [2].

Small animals use numerous mechanorceptors in their legs and feet to monitor foot/ground interactions and adjust their gait and speed accordingly. For example, in insects, campaniform sensilla and sensory hairs provide a dynamic measure of contacts and loads in the limbs [3]. However, practical considerations including sensor size, robustness and wiring have made it difficult to equip small robots with anything approaching the sensory capabilities of small legged animals. Tactile sensing on the feet would allow small robots to sense the magnitudes and locations of ground contacts, providing a measure of stability and maneuverability. It could also allow robots to identify the terrain type and perform gait adjustments for more efficient locomotion.

Among tactile sensors, capacitive sensors have enjoyed a recent increase in popularity due to the availability of inexpensive surface-mounted capacitance to digital converters (CDCs) to provide active shielding, signal processing and digital communication. Examples include sensors for robot hands [4], [5] and miniature surgical grippers [6], [7]. For ground reaction force sensing in small legged robots, capacitive tactile sensors based on flexible circuits with surface-mounted CDCs are attractive due to their low weight, robustness, and ability to wrap around various geometries. For robots with rotary legs, the minimization of wiring is an additional advantage.

In this paper, we study the utility of capacitive sensors on small robot legs in measuring ground interactions and updating adaptive gaits for different terrains. We present the design and performance characterization of a thin, flexible capacitive sensor designed to capture spatially distributed tactile forces on a curved robot leg. To select appropriate gaits, we examined running performance on different terrains, such as hard surfaces, grass and granular media. A machine learning classifier uses tactile sensor features in conjunction with motor information to identify terrain type with 82.5% accuracy. The main source of error is difficulty in distinguishing between hard surfaces with high or moderate friction. In adaptive gait tests on a transition between terrains, we show that terrain-based gait adaptation improves the locomotion speed by 17.1% and reduces cost of transport by 13.2%.

II. Related Work

A. Tactile Sensing for Robotic Locomotion

Many technologies are potentially applicable to ground force sensing including force/torque and tactile sensors. Common concerns include size and weight, especially on small robots, and the complexity of wiring to connect the foot to the body.

One of the earliest examples of tactile sensing in robotic locomotion is the Raibert hopper [8], [9] which included a binary ground contact sensor. Recognizing that binary contact information is not enough to plan gaits and maintain control on irregular terrain, other early legged robots used force sensing [10], [11].

On large robots, force/torque sensors at the ankle are popular. They measure dynamic ground forces directly, and their weight and volume are not difficult to accommodate. However, they must be robust as they are subject to repeated impacts. Many humanoid robots incorporate F/T sensors at the ankles to measure forces and moments associated with maintaining balance and sense ground reaction forces (GRFs) [12]–[16]. For the running Cheetah robot, Chuah et al. [17] present a light and robust foot sensor. Kuehn et al. [18] present a design for the foot that combines force/torque, tactile, acceleration and proximity sensing.

*These authors contributed equally to this work.

All Authors are with Mechanical Engineering Dept., Stanford University. BDML at Center for Design Research, 424 Panama Mall, Bldg. 560, Stanford, CA 94305-2232 taemyung at stanford dot edu

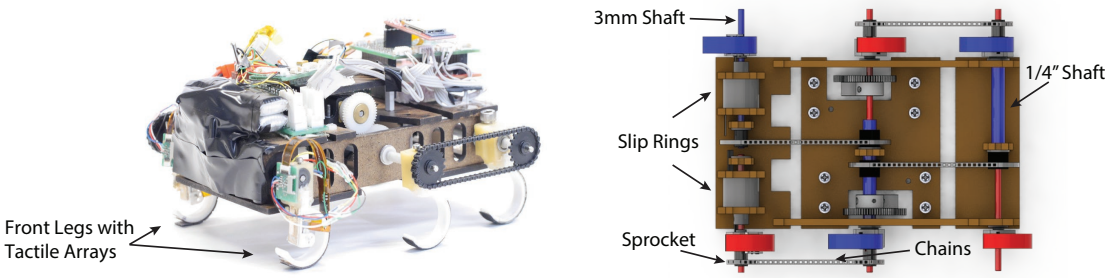

Fig. 1: Photograph and rendering of underside of SAIL-R, a hexapod drived by two motors in an alternating tripod gait. Slip rings transmit power and communications to the tactile arrays on the front feet.

With tight constraints on volume and weight, force/torque and tactile sensors are much less common in small legged robots. However, these robots may more affected by the details of foot/ground interaction when dissipative effects scale with area rather than mass. Early efforts again include binary contact sensors [19]. More recent demonstrations include binary hair arrays, body tactile bumpers, and leg strain sensing [20], [21].

The requirements to equip the feet of a small robot with tactile sensors are similar to those for a dexterous hand, although contact rates are higher (requiring a faster sampling rate and higher mechanical bandwidth) and average forces may be lower. Many transduction methods are possible including optical, magnetic, piezoresistive, piezoelectric and capacitive. Tactile sensing reviews are provided in [22]–[25]. A particular wiring and communication challenge is introduced when the robot legs undergo continuous rotation as in EduBot [26], Whegs [27], and the robot in this paper.

Among possible transduction methods, piezoresistive sensors based on conductive inks or polymers are inexpensive and compact. However they typically suffer from substantial hysteresis, which limits their use for dynamic applications [24]. Another possibility is to pattern strain gages directly onto the feet [20], but this solution requires signal conditioning circuits and presents challenges for wiring between continuously rotating legs and the robot body. As noted earlier, capacitive sensors are increasingly popular; recent examples include [28]–[32].

The main contribution of this paper is that it demonstrates utility of distributed tactile sensing on the feet of a small robot to identify terrain types and adjust gait accordingly. To our knowledge, it also presents the first small (<500 g), untethered robot with rotary legs and tactile sensors that measure shear and distributed normal forces at the feet. Using the sensors, we identify features useful to distinguish among terrain types, allowing the robot to automatically adjust its gait for increased speed and efficiency.

B. Gait Adaptation and Terrain Identification

Animals use a combination of neural feedback and passive mechanical properties to accommodate variations in terrain, the former being more observable in higher animals (e.g. mammalian running [33]–[35]) and the latter in running arthropods [36], [37].

Gait adjustment may consist of variations in timing [38], leg stiffness and swing angle or it may require a more dramatic change, for example when transitioning from a hard surface to granular media [39]. Strategies have included modifying a wave gait based on inertial measurements and proprioceptive information [40]; varying the parameters of a CPG-based controller [41], [42], and varying the phase of a feedback control [43]. For Rhex robots, gait tuning [44] and gait transitions were demonstrated, for example to switch from floors to stairs [45].

Terrain identification has also been an important topic for wheeled-autonomous vehicles. Sensing methodologies include dynamic vibration signals from inertial measurement units (IMUs) [46]–[48], current/voltage measurements from motors [49]–[52], vision systems [53]–[57], sound [58], and dynamic tactile probes [59].

Although terrain identification for legged robots is less developed, several approaches have been demonstrated using a combination of contact and non-contact sensing. For large robots, the dynamic signals from force/torque sensors [60], [61], and tactile arrays [62]–[64] have been used. Indirect sensing, such as motor current/position sensing and IMUs in the robot body, is also used for terrain identification or classification algorithms [65]–[70].

For small running robots, however, indirect sensing has a couple of disadvantages for characterizing ground contacts. Motors may have a substantial gear ratio and may drive multiple legs. Hence motor current is a relatively insensitive dynamic measure of force variations at, for example, the front feet. In addition, body inertial measurements are noisy, especially when running on rough surfaces, and body accelerations reflect the impulses from multiple feet; this requires longer episode lengths (sensor sampling time for averaging statistical features) to obtain higher accuracy [66].

The terrain identification approach used here extends that presented in [32] for a planar hopper by incorporating spatially distributed temporal ground contact force data from an untethered hexapod for terrain classification. Details of the terrain classifier are presented in Section IV-E.

III. SAIL-R

A. Robot Design

SAIL-R (Fig. 1) is a hexapod with C-shaped legs, intermediate in size between EduBot [26] and DynaRoACH [71]. The chassis is constructed of laser-cut masonite and the legs are

3D-printed ABS plastic. Robot specifications are provided in Table I.

1) Transmission System: Chain and sprocket transmissions link the two motors (Pololu 50:1 Micro Metal Gearmotor) to the left and right tripods, shown red and blue in Fig. 1. The overall gear ratio is 65:1 from the motors to the legs. Encoders provide a resolution of 0.46° at the legs. Slip rings (Orbex Group, 503-0600) on the front legs transmit power and communications to the tactile sensors.

2) Control Electronics: The controller is a 32-bit ARM® Cortex®-M4F microprocessor (TI TM4C123GH6PM). Additional components include a current and voltage sensor (Attopilot, 13.6 V/45 Amps), motor drivers (TI DRV8838), voltage regulator (TI TPS63061), Bluetooth radio modem (Roving Networks RN-42), and the tactile sensors, which are described in Section III-C1. The main control loop runs at 333 Hz.

B. Gait Control

There are various ways of generating and controlling the gait of a hexapod robot. A review on the dynamics and stability of legged locomotion can be found in [72]. In particular, central pattern generators (CPGs) (a survey of which can be found in [73]) are a standard tool to design gait reference generators.

However, one of the goals of the present work is to use ground reaction force information to help a robot determine appropriate gait parameters for a particular type of surface. In this respect, a disadvantage of CPGs is that model parameters such as the type and number of oscillators, waveform parameters such as frequency, amplitude and phase lag, and the effects of input and feedback signals, are strongly interconnected. As a result, it is difficult to change gait patterns without continuously solving sets of coupled differential equations online. This challenge is exacerbated by the lack of well-understood dynamic models for leg-ground interaction for hybrid wheel-leg robots traversing deformable and granular surfaces such as grass and sand.

Alternatively, the Buehler clock gait kinematics described in [74] provide a tested framework to relate the stance and air-borne gait phases of a hexapod robot with hybrid wheel-legs. This generator ensures gait stability and enables the robot to traverse a variety of outdoor terrain by tuning four control parameters: t_c the cycle period, t_s the stance time, ϕ_s the stance phase angle, and t_d the double stance time when both tripods are contacting the ground. An illustration of this phase-based gait cycle is provided in Fig. 2. The Buehler clock gait tuning allows simple exploration of various gaits and smooth

TABLE I: Specifications for hexapod robot.

Parameter (μ)	Value	Units
External Dimensions (LxWxH)	140x80x30	mm
Mass	375	g
Leg length	38.5	mm
Leg stiffness	3400	N/m
Motor stall torque	105.9	mNm
Motor no load speed	625	rpm
Gear ratio	65:1	

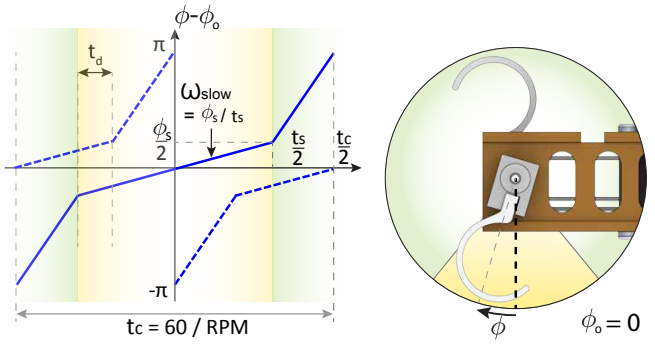

Fig. 2: Buehler clock gait cycle [74] features include ω_{slow} (slope of ϕ_s over t_s) and RPM. Green shaded region is fast portion of gait, yellow is slow.

gait transitions. For similar reasons, others [69] have also used the Buehler Clock for gait adaptation. Here, we define ω_{slow}, the angular velocity of leg rotation during stance phase, as ϕ_s/t_s and we vary t_c by the leg RPM. In Section IV-B we explain the choice of gait parameter sets for exploring how changing a single control parameter can lead to different locomotion performance on different surfaces.

C. Tactile Sensing

1) Sensor Design and Integration: The capacitive sensor design (Fig. 3) is adapted from [32] and consists of five 5x5 mm normal force sensing taxels along an 8 mm wide polyimide four-layer flex circuit (FPCB). An additional taxel, sandwiched in a preloaded elastic hinge at the hub, measures the overall shear force. The circular leg design decouples shear and normal force measurements. Normal forces, which are directed radially inward on the legs, produce very little moment at the center and hence are not measured by the shear force sensor; in contrast, tangential forces produce large moments and load the shear force sensor in compression and tension. The sensor is bonded to a 3D-printed (Stratasys ABSplus) curved robot leg (10mm wide, 40mm long measured from hip to toe) with adhesive (Loctite 401). The total sensor/leg assembly mass is 2.89 g, of which the sensor is 1.14 g.

A 16-bit CDC (Analog Devices AD7147) samples the six sensing pads at 217 Hz. Sensor data are acquired via I2C through a microcontroller (Microchip PIC24F04KA201) and sent to the main robot microcontroller through UART.

2) Sensor Performance: The curved sensor/leg assembly is calibrated against a commercial force/torque sensor (ATI Gamma SI-32-2.5, accuracy: 0.05N) while mounted to the body of the robot. Fig. 4 shows calibrated sensor data in normal and shear axes as compared to the ATI load cell. The calibration takes bending of the leg into account to maintain decoupling of normal and shear forces at the contact, and demonstrates a close match to ATI load cell data. As in [32], the minimum resolvable normal force is ≈13 mN. Although the sensor been tested for loads of 100 N in compression, in practice the maximum force is approximately 15 N in both normal and shear directions to avoid damaging the legs.

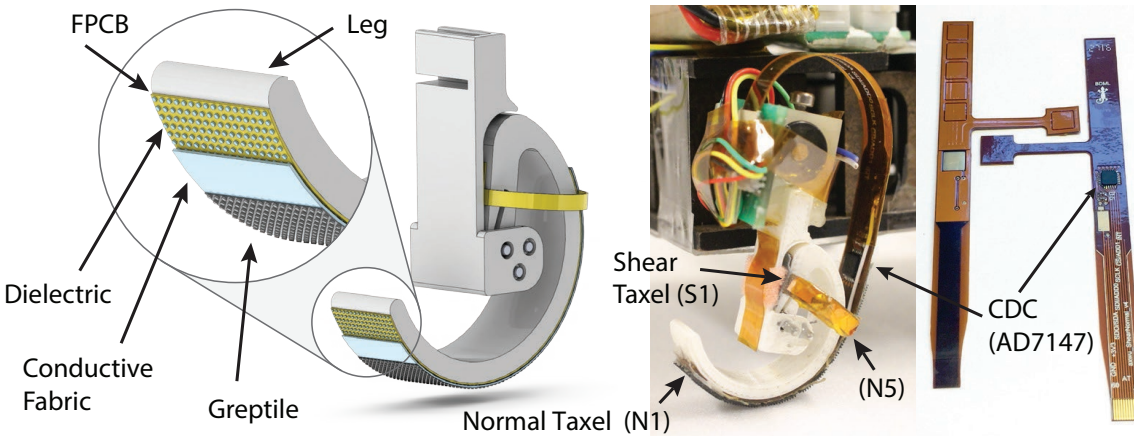

Fig. 3: Integrated capacitive tactile sensor on the front legs: five normal force taxels are along the contact region of the leg; a sixth taxle at the hub measures shear forces. 3D printed ABS leg is coated with 3M *Greptile*™ for traction.

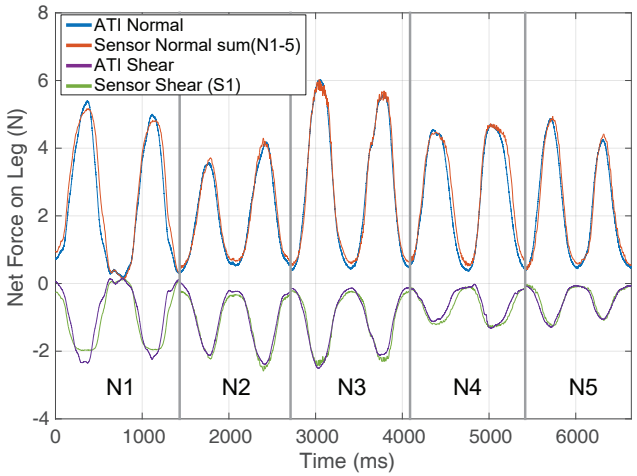

Fig. 4: Comparison of tactile sensor output vs. ATI load-cell for shear/normal force loading. Positive force is in compression for normal taxels and forward traction for the shear taxel. Each segment represents a contact point of a normal taxel.

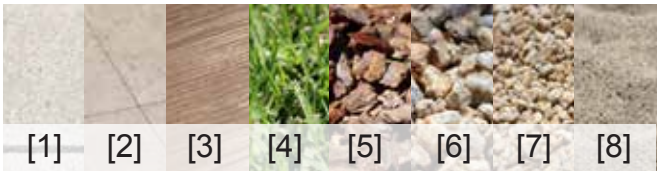

Fig. 5: Outdoor terrains with varying physical properties selected for gait experiments.

IV. Gait Adaptation for Different Terrains

We studied gait adaptations for faster and more efficient running on different types of terrain. First, we examined performance on different terrains to select desired gait parameters.

A. Terrain Selection

As shown in Fig. 5, eight outdoor surfaces with varying stiffness, friction, and dissipation were considered for gait selection and terrain classification. Surface properties are summarized in Table II. As in [32], the surfaces are grouped into classes: high friction, high stiffness (HF), low friction, high stiffness (LF), deformable (D), and granular (G).

TABLE II: Terrains used in GRF sensing and classification. Numbers match Fig, 5; machine learning class labels listed in Section IV-A.

Terrain	Description	Friction Coefficient (μ)	Penetration Depth (mm)	Class Label
1	concrete	1.0	0	HF
2	waxed tile	0.5	0	LF
3	laminate wood	0.6	0	LF
4	medium-density grass	1.14	20	D
5	wood chips/mulch	1.04	7	D
6	gravel	1.04	5	D
7	pebble	0.88	8	D
8	sand	0.95	25	G

B. Viable Gait Parameter Space

On different surfaces, we explored two gait patterns: fast-walk and trot. In general, the gaits with a longer ground contact time would be considered walk or fast-walk gaits and those with a short ground contact time would be considered trots.

For fast-walk gaits, we varied the overall leg rotation speed (RPM) while holding the ground contact time (t_s) and ϕ_s fixed. For most of these gaits there is a significant double-stance time as a fraction of the overall gait period. The Buehler clock parameters for this series are illustrated in Fig. 6a with leg speed varying from 260 to 320 RPM.

For gaits approaching a trot, we varied ω_{slow} while holding the overall leg rotation speed and ϕ_s fixed. As ω_{slow} increases, the ground contact time becomes shorter, and the gait becomes increasingly impulsive, approaching a trot with an airborne phase. The Buehler clock parameters for this series are illustrated in Fig. 6b with the ω_{slow} varying from 7.6 to 30.3 rad/sec and the overall leg cycle fixed at 260 RPM.

For both series, the upper limit on overall rpm or ω_{slow} is limited by the need to avoid damage to the legs on hard surfaces.

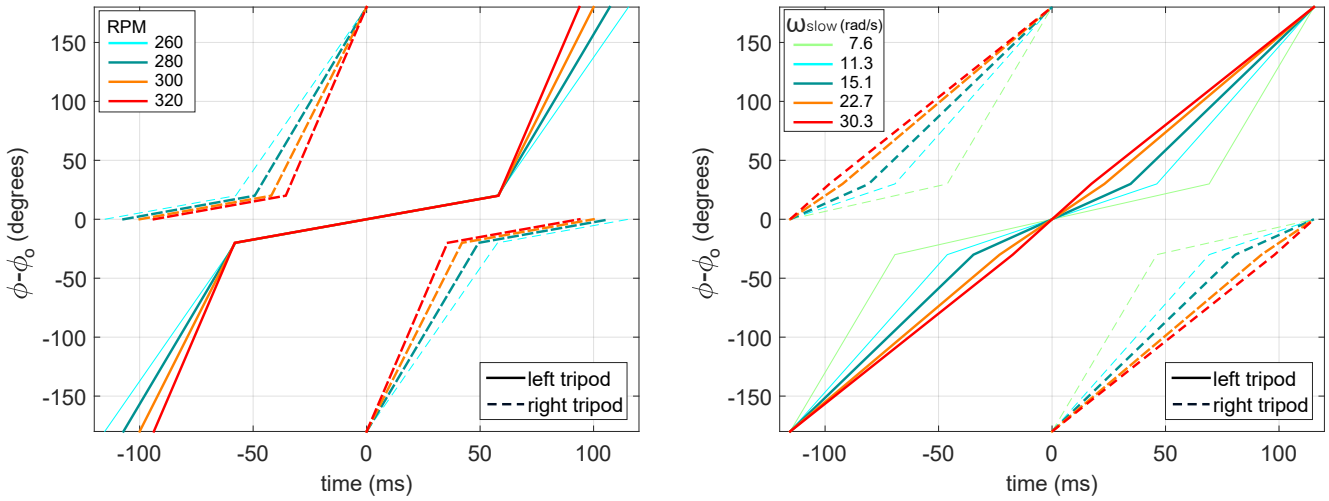

(a) Fast walk (ω_{slow} = 6.0 rad/s, ϕ_s = 40deg)

(b) Trot (RPM = 260, ϕ_s = 60deg)

Fig. 6: Buehler clock gait parameters for testing two types of locomotion behavior: (a) fast walk and (b) trot. Bold lines are gait parameters with faster body speeds.

TABLE III: Preferred gait selection on different terrain

	v (Body Speed)	COT	Leg Structural Safety
HF	Fast walk	Fast walk	Fast walk
LF	Fast walk	Fast walk	Fast walk
D	Trot	Trot	Trot $\approx$ Fast walk
G	Fast walk	Fast walk	Trot $\approx$ Fast walk

C. Locomotion Results

For both fast walk and trot gaits, we ran SAIL-R five times with each set of gait parameters. High speed videos (240 FPS) were recorded to observe leg-ground interactions; example videos on each class of terrains are included in the supplementary material. We evaluated two performance metrics: forward velocity and cost of transport (COT) or specific resistance, calculated as $S = P_e/mgv$, where P_e is the total electrical power of the system, g is the gravitational constant, and v is the forward velocity. The forward velocity is measured by allowing the robot to perform open-loop free running given a set of gait parameters for 5 s and taking the distance between the starting and ending positions. Five trials were performed for each set of gaits; results are shown in Fig. 7 and 8. Table III lists comparisons between fast walk and trot gaits on each type of terrain. The detailed explanation is as follows.

1) Hard Surfaces (HF, LF): On hard surfaces, the robot performs with better repeatability and smoothness (i.e., repeated stride to stride landing, and small body roll and pitch motions) when using a fast walk than a trot. To avoid potential leg damage, the robot is unable to exceed ω_{slow} of 11.3 rad/s in the trot gait. A further discussion of safety to avoid leg damage is provided in Section IV-D1.

Body speeds generally increase as the stride frequency increases. On concrete, however, Fig. 7a shows a slight decrease in speed at 320 RPM. With this high stride frequency, the robot gaits become erratic with impulsive leg-ground contacts, lowering the forward body speed. Due to slippage, LF (laminate) shows lower speeds than HF (concrete).

Cost of transport generally decreases with increased stride

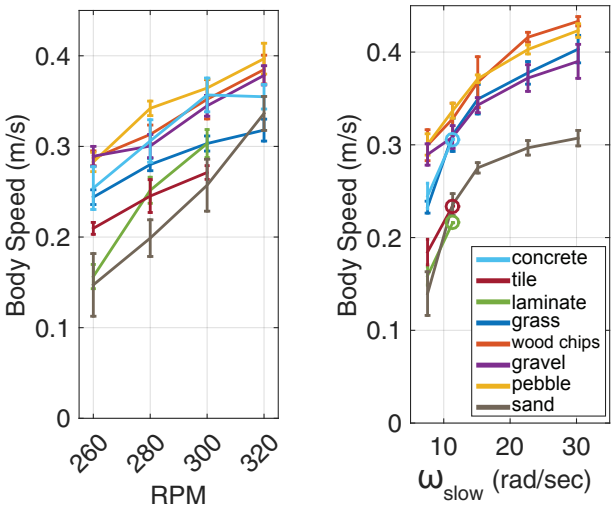

(a) Fast walk gait

(b) Trot gait

Fig. 7: Forward robot velocities achieved with (a) fast walk gait and (b) trot gait.

frequency due to the increased body speed with bouncing gait behavior (Fig. 8a). With stable fast walk gaits (260 RPM), LF (tile, laminate) has slightly higher COT than HF (concrete) because of the slip. With more aggressive fast walk gaits (RPM $\geq$ 280), HF and LF have a comparable COT and the ground interactions on both terrains are mostly impulsive normal contacts.

2) Deformable Surfaces (D): Both fast walk and trot gaits are consistently smooth and predictable on deformable surfaces (D) such as wood chips, gravel, pebbles and grass. Body speeds increase with stride frequency or ω_{slow}. With the given control, Fig. 7b shows that the trot gait at 260 RPM can achieve higher speed than fast walks; we observe fast "crawling" behaviors with trot gaits, pushing off harder against the deformable terrain despite significant penetration depths.

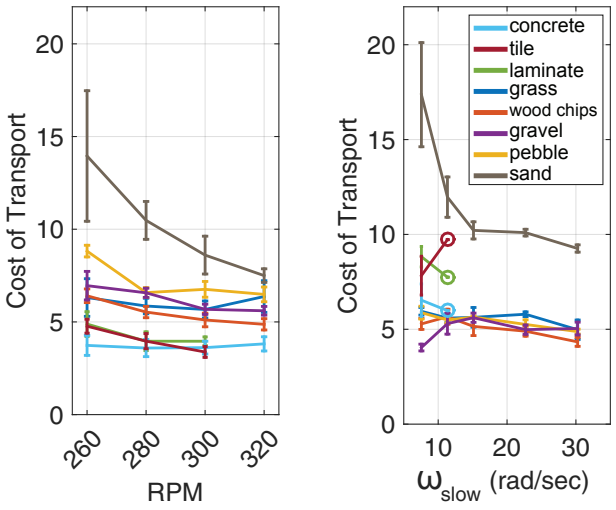

(a) Fast walk gait (b) Trot gait

Fig. 8: Robot cost of transport (COT) achieved with (a) fast walk gait and (b) trot gait.

Costs of transport for fast walks are slightly higher than trot gaits, but they are comparable. We observe that both types of gaits run with high penetration depths on D, requiring high motor torques and power consumption.

3) Granular Media (G): Both fast walk and trot gaits are comparatively stable because the particles dissipate impact energy. Fig. 7 shows both gaits with comparable body speeds. In contrast, prior work with SandBot found that a double stance (both tripods in contact with ground), which occurs with fast walk gaits, significantly lowers the body speed on G because of interference between the tripods [1]. The result may stem from the difference in weight: SAIL-R is 6 times lighter than the 2.3 kg SandBot and has less surface penetration.

Fig. 7 also shows a monotonic increase in speed without any decreases due to transitioning into swimming [1]. Again, the low weight of SAIL-R generates sufficient lift to prevent such a transition [2].

Comparing the fast walk and trot gaits, the former has a higher maximum speed with lower COT; we surmise that in the double-stance phase, the two tripods push the terrain with lower foot pressure for less energy loss. More generally, among all surfaces, G shows highest COT in both gaits because the robot does not have an airborne period.

D. Ground Reaction Forces vs. Gait

Normal and shear ground reaction forces across the 8 surfaces tested are shown in Fig. 9. As expected contacts on harder surfaces are more impulsive. On deformable surfaces and sand, ground contacts result in lower maximum normal force and a longer period of contact. Shear sensor signals are more pronounced on deformable surfaces and resemble the spring-inverted pendulum (SLIP) model of dynamic legged locomotion [75]. However, deviations from the model can be seen on surfaces such as gravel, wood chips, and pebbles. We believe this may be caused by the foot displacing material.

1) Gait Consistency and Safety Analysis: Tactile sensors also provide valuable information about gait quality. Especially on hard surfaces, a smooth and predictable gait without substantial rolling and pitching gives more consistent contact locations. From experiments, we located the leg contact points by monitoring normal sensor indices (N1-5) where the maximum force occurs during each step (900 steps for both HF and LF). Fig. 10 shows that the sensor index varies more with aggressive gaits, meaning more inconsistent landing locations of the legs.

By combining measured normal force data with Buehler clock phases, we can further evaluate the consistency of each step (Fig. 11). For example, in a delayed landing step, the robot lands as it transitions into the faster portion of its gait cycle, resulting in undesired locomotion. Missed ground contact in a cycle indicates an airborne behavior of the leg, causing uneven load distribution on the other legs and potential leg failure.

By monitoring the measured force level and missed steps, the robot can examine gait safety to avoid structural failures. Fig. 12 shows peak normal forces of each step and the ratio of missed steps from 8200 strides. On hard surfaces (HF, LF), both fast walk and trot gaits demonstrate similar GRFs. However, trot gaits show significantly more missed steps, making them less safe for the legs. On soft surfaces (D, G), the GRFs are lower than for hard surfaces because the media dissipate impact energy. Although trot gaits shows few missed steps due to the heterogeneity of the terrain, lower GRFs ensure the legs will still be safe from damage.

2) Distributed Tactile Sensing: Figure 13 demonstrates spatially distributed GRF data as measured by the tactile sensor. As in [32], the sensor is able to track contact forces at various points along the legs. On softer surfaces, contact duration is longer for each step while amplitude is smaller. Contact locations are also noticeably different; hard surfaces have a single contact point, D shows sequential contact point changes, and G shows shared loads on multiple contact points. These measurements provide confidence that contact force signatures are unique to surface types and that temporal information from the sensor can be useful in terrain identification.

E. Outdoor Terrain Classification

Tactile sensors were used to classify outdoor terrains. For comparison with previously reported approaches [66], we also mounted an IMU to the robot and used it to classify terrains.

1) Features Extraction: For the tactile sensors of SAIL-R, we extract relevant features from single-stride sensor waveforms. Table IV provides a list of features used for the classifier. For comparison, we also attached a 6 DOF IMU (ITG3200/ADXL345), sampled at 200 Hz. The extracted features from the IMU experiments are listed in Table V and are similar to [66]. For comparison, the episode length is chosen as 50 ms (average single stride contact duration) around the local peak of vertical accelerations.

2) Classifier Selection: To evaluate the machine learning performance of terrain classifications, we used a support vector machine (SVM) classifier with a PUK kernel because of its high accuracy in terrain classification when used previously on

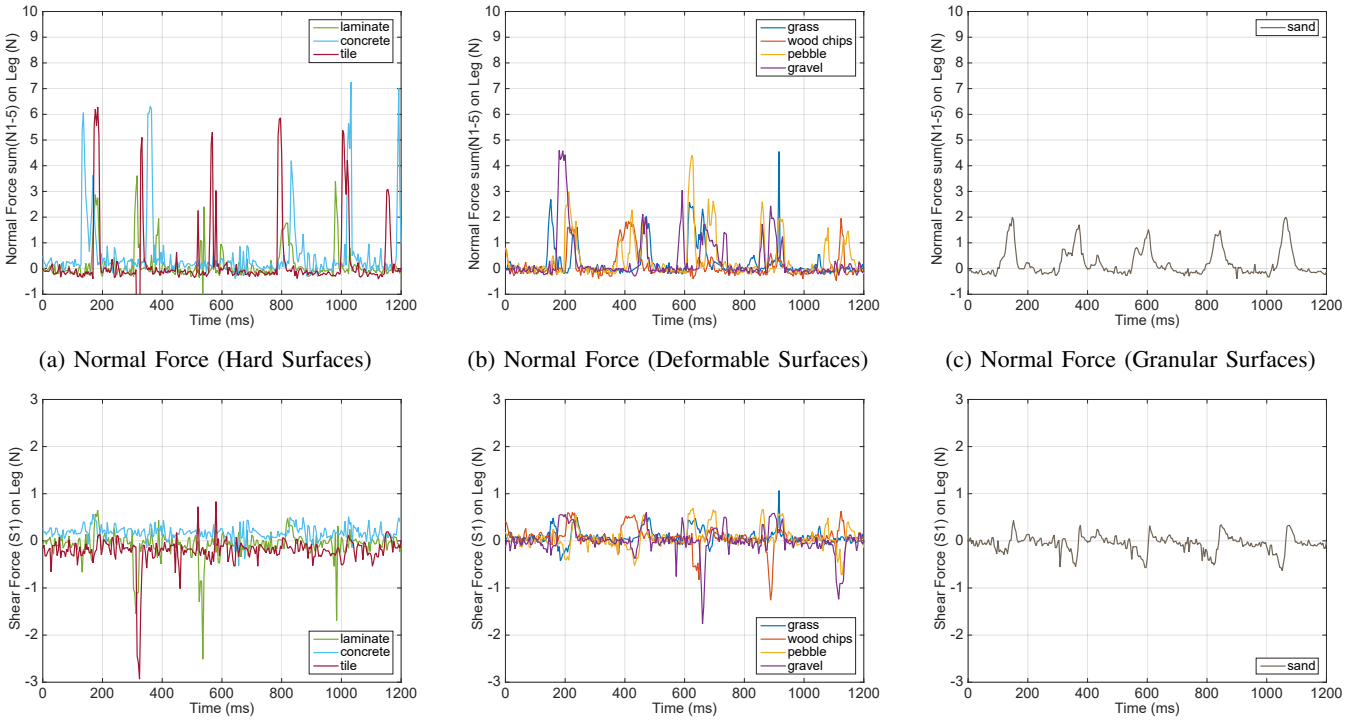

(a) Normal Force (Hard Surfaces) (b) Normal Force (Deformable Surfaces) (c) Normal Force (Granular Surfaces)

(d) Shear Force (Hard Surfaces) (e) Shear Force (Deformable Surfaces) (f) Shear Force (Granular Surfaces)

Fig. 9: Typical normal and shear forces captured during locomotion on selected surfaces. Gait Parameters for Hard surfaces (a, d) are fast walk with RPM = 280. In other cases(b,c,e,f), gait parameters are for a trot with $\omega_{slow} = 11.3$ rad/s

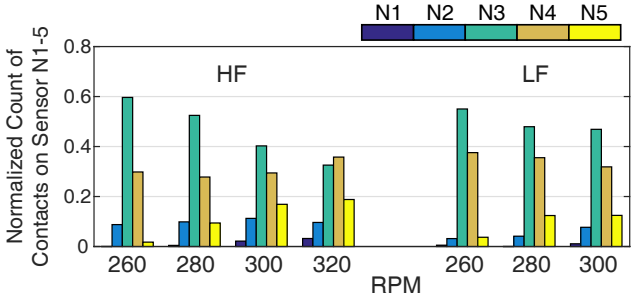

Fig. 10: Distribution of leg contact locations on HF and LF with fast walk gaits.

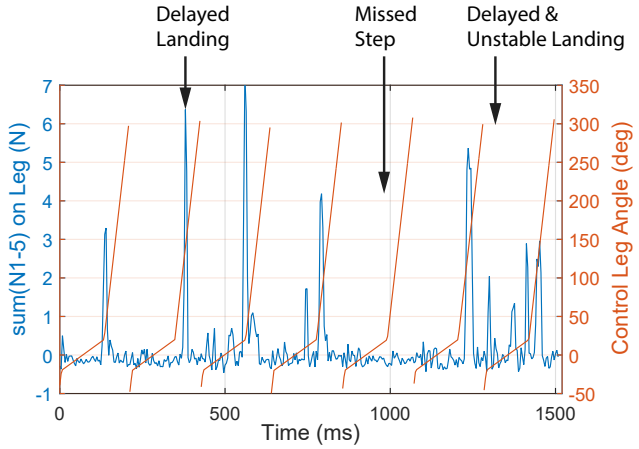

Fig. 11: Normal force on legs compared to control leg angles for consecutive unstable strides on a single leg. Testing surface is HF.

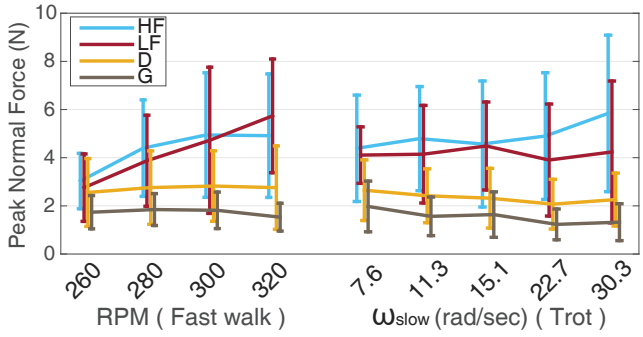

(a) Peak normal force per each step

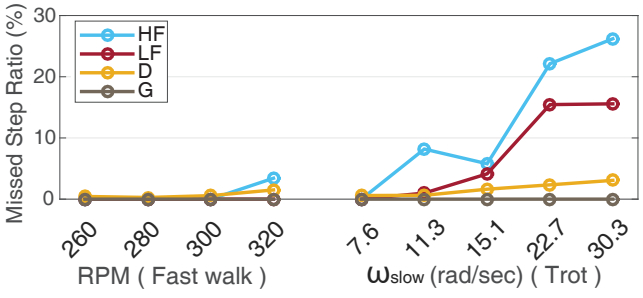

(b) Missed step ratio

Fig. 12: Metrics for gentle and consistent ground contacts: (a) Peak normal forces measured per each step and (b) Ratio of missed step counts to commanded step counts

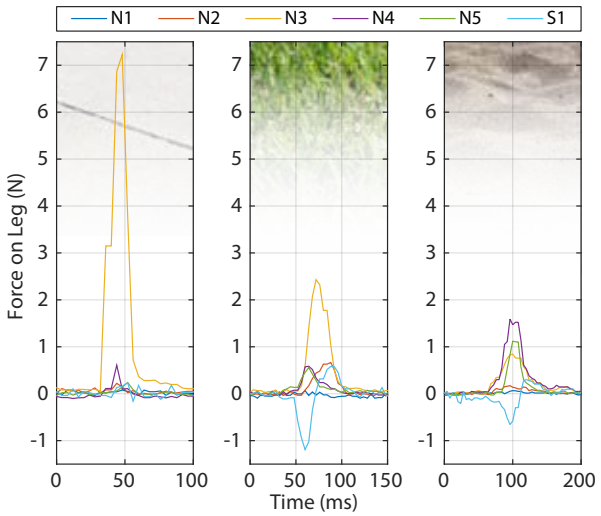

Fig. 13: Distributed tactile sensing on a C-leg across various surfaces (from left: concrete, grass, sand), where N1 represents the most distal taxel on the tip of the leg, N5 the most proximal taxel near the hip, and S1 the shear signal.

TABLE IV: Tactile Machine Learning Feature Set (*excluded for real time classification in Section IV-F)

Index	Feature Name
1	Peak amplitude of sum(N1-5)
2	Contact period of sum(N1-5)
3	Area under curve (impulse) of sum(N1-5)
4	Gait parameter - Motor RPM
5	Gait parameter - Ratio Ts to Tc
6	Average amplitude of sum(N1-5)
7	Gait parameter - ω_{slow}
8-12	Individual normal taxel (N1-5) force peak amplitude
13-17	Individual normal taxel (N1-5) rise time to peak
18-22	Ratio of individual taxel force peak to peak sum(N1-5)
23-25	Max, min, average shear taxel force (S1)
26*	Motor RPM at peak sum(N1-5)
27*	Input current at peak sum(N1-5)
28-29*	Input current average, range
30-34	Average normal force on individual taxels (N1-5)
35-39*	Motor RPM at peak force for individual taxels (N1-5)

TABLE V: IMU Machine Learning Feature Set

Index	Feature Name
1	Gait parameter - Motor RPM
2	Gait parameter - Ratio Ts to Tc
3	Gait parameter - ω_{slow}
4-12	2^{nd} statistical moment of two motor RPM, acceleration (x,y,z), angular velocity (x,y,z), input current
13-21	3^{rd} statistical moment of the same features
22-30	4^{rd} statistical moment of the same features

a bipedal platform in [32]. For both tactile sensor and IMU features, a total of 3072 data sets (768 per terrain class) were used to train and test the classifier. WEKA 3.7 [76] was used for classifier training and testing. Table VI lists the classifier accuracy evaluated using 10-fold cross-validation.

3) Classifier Performance: Using the tactile sensing features in Table IV, the SVM classifier achieved 82.5% overall accuracy. Notably, the accuracy was 25% worse for distinguishing hard high friction (HF) and low friction (LF) surfaces. This is partly because the coefficients of friction, $\mu \approx 1$ for

TABLE VI: SVM classifier results using feature set of Table IV and Table V.

		Predicted Class							
		HF		LF		D		G	
		Tactile	IMU	Tactile	IMU	Tactile	IMU	Tactile	IMU
True Class	HF	69.8%	58.1%	28.9%	32.6%	0.9%	5.6%	0.4%	3.8%
	LF	28.5%	26.6%	69.8%	61.9%	1.0%	7.9%	0.7%	3.7%
	D	3.0%	5.7%	1.2%	5.7%	92.5%	73.1%	3.4%	15.5%
	G	0.4%	0.3%	0.1%	1.2%	1.7%	6.5%	97.8%	92.1%

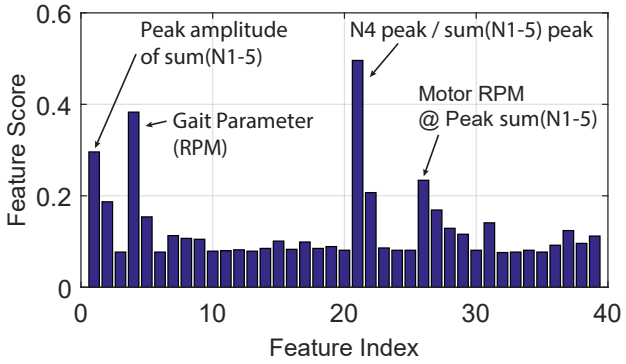

Fig. 14: SVM classifier weight of features in Table IV

HF and $\mu \approx 0.5$ for LF, are much closer than in previous work [32], where the coefficient of friction was $\mu = 0.04$ for the LF surface. Hence the contact forces for the HF and LF cases are relatively similar. A second issue is that the most useful signal for friction is the shear force, but we observe from Fig. 9f that the quality of the shear data for hard surfaces is relatively poor due to the short contact time. A better solution in the future is probably to model hard surfaces as having a spectrum ranging from low to high friction, with each tested surface occupying an approximate place along the spectrum.

When comparing classification using tactile versus IMU features, we observe that the tactile features are particularly effective on deformable surfaces. On average, the accuracy is 11% higher, and for deformable surfaces (D) it is 19% higher. With IMU data, there is a noticeable confusion between D and G; we surmise that both surfaces stabilize the body motions by absorbing impact energy, making the differentiation harder. However, as shown in Fig. 13, tactile sensors provide distinguishable temporal and spatial information which easily differentiates D from G.

A potential advantage of tactile sensing is a short episode length. Table VI shows that the overall performance is better in tactile sensing features with the comparable episode lengths (average 41ms for tactile features and 50ms for IMU features). As mentioned in [66], the statistical moment approach, which is used for IMU feature sets, requires a longer episode for better accuracy; we surmise that it takes longer to develop distinguishable vibratory patterns of body motions. In contrast, the tactile sensor measures the GRF as it makes contact.

4) Feature Analysis: To examine the value each tactile feature adds, we performed feature score analysis on the SVM classifier using a greedy stepwise search algorithm. Fig. 14 shows that among the top 4 features, two (21, 1) are directly related to GRF measurements from tactile sensors and one (26) uses the temporal information of tactile sensing. One of

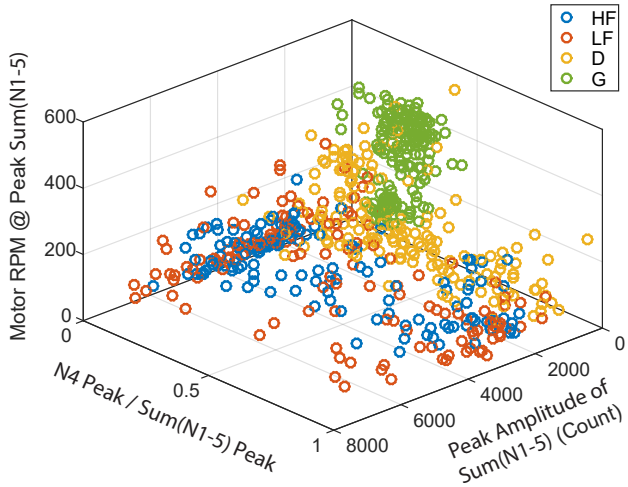

Fig. 15: Class distribution plot with four most attributing features of SVM classifier. Motor RPM = 260.

TABLE VII: Logistic classifier results using a feature set of Table IV without motor measurements

		Predicted Class			
		HF	LF	D	G
True Class	HF	67.3%	28.0%	2.1%	2.6%
	LF	28.1%	66.8%	2.5%	2.6%
	D	5.0%	2.7%	73.2%	19.1%
	G	1.0%	0.7%	14.1%	84.2%

TABLE VIII: Surface Specific Adaptive Gait Parameters

Terrain Class	RPM	t_s/t_c	ϕ_s (rad)	ω_{slow} (rad/s)	Gait Type
Sampling	240	0.47	0.7	6.0	slow walk
HF	300	0.58	0.7	6.0	fast walk
LF	280	0.5	0.7	6.0	fast walk
D	260	0.3	1.05	22.7	trot
G	300	0.58	0.7	6.0	fast walk

the gait parameters (RPM) scored the second highest because it varies the locomotion significantly [66].

Fig. 15 demonstrates qualitatively how the top 4 features classify the terrains. The proportion of N4 to the normal force sum (Index 21) shows semi-binary distributions on hard surfaces (HF, LF), wide distributions on D, and concentrated distributions on G. These patterns follow the characteristics of each terrain: hard surfaces give impulsive single point contact (usually on N3 or N4), deformable surfaces give non-uniform distributed contact, while G has a more uniform or consistent contact. Peak amplitudes of normal force sum (Index 1) mostly differentiate hard and soft terrains because soft terrain dissipates impact energy more. Motor RPM at peak of normal force sum (Index 26) mostly differentiates D from G because of the difference in penetration depth.

F. Real-Time Terrain Classification and Gait Adaptation

In this section we present adaptive gait control based on real-time terrain classification using tactile sensors; example videos are included in the supplementary material.

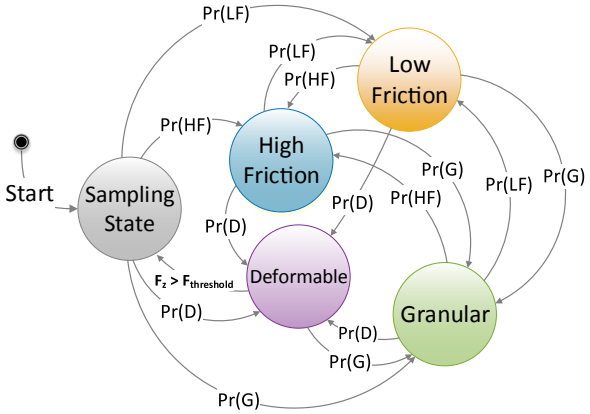

Fig. 16: FSM implementation of terrain-based gait adaptation based on the cumulative probability calculated by the logistic regression classifier. $Pr(x)$ represents the highest cumulative probability for a particular surface type.

1) Real-Time Terrain Classification: The SVM classifier uses between 500-600 support vectors for each stride instance, which requires more computational effort than a logistic classifier. Comparatively, the logistic classifier model can be evaluated with a single line of C code. Due to SAIL-R's computational limitations, we concluded that the logistic classifier is a better candidate for real-time terrain classification.

To further reduce computational effort, we used only the left leg sensors and a subset of the features, flagged with an asterisk in Table IV. In this case the overall accuracy decreases to 72.9% (Table VII). Again the main confusion is between HF and LF surfaces. To compensate for the reduced overall accuracy we implemented a real-time classification algorithm that takes into account the history of prior steps to create a weighted cumulative probability.

The probability of being on j^{th} terrain (P_j) from the multinomial logistic classifier model [77] is:

$$P_j(x^{(n)}) = \frac{e^{\beta_j^T x^{(n)}}}{1 + \sum_{j=1}^{k-1} e^{\beta_j^T x^{(n)}}} \qquad (j = 1, \cdots, k-1)$$

$$P_k(x^{(n)}) = 1 - \sum_{j=1}^{k-1} P_j(x^{(n)}) = \frac{1}{1 + \sum_{j=1}^{k-1} e^{\beta_j^T x^{(n)}}} \qquad (1)$$

where k is the number of terrain classes, $x^{(n)}$ is a feature vector of the n^{th} stride instance, and β_j is a coefficient vector of the logistic classifier for j^{th} class. The weighted cumulative probability(CP) for each terrain class is then:

$$CP_{n,j} = P_j(x^{(n)}) + \alpha CP_{n-1,j} \qquad (2)$$

where α is the weight factor (< 1). The final terrain type is selected by the class with the highest cumulative probability.

This algorithm adds robustness for lower accuracy surfaces, e.g. between HF and LF, but slows the response. For gait adaption, the detection delay, which can be tuned by α, should be selected based on the application. A large (conservative) α value increases accuracy at the cost of response time, but a small α can lead to unstable robot performance caused by frequent changes in gait parameters.

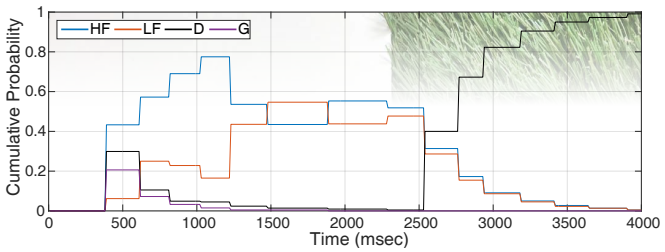

(a) Normalized cumulative probability

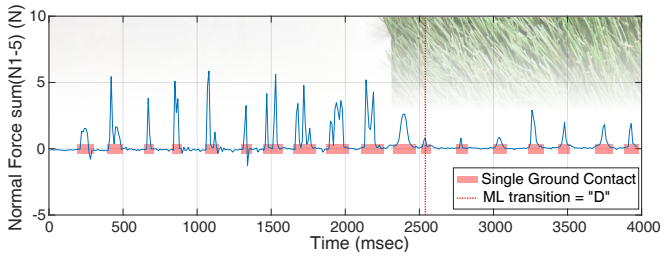

(b) Normal force sum (N1-5) of one leg

Fig. 17: Real-time terrain identification results based on logistic classifier and cumulative probability ($\alpha = 0.7$). The classifier used information from one step to classify the transition.

(a) Traversing high-friction and deformable surfaces with a steady fast walk.

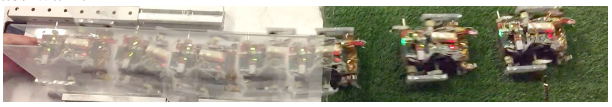

(b) Traversing a high-friction surface with a fast walk and transitioning to a trotting gait on a deformable surface.

Fig. 18: Adaptive gait control demonstrating improved speed. Frame interval is 520 ms; increased distance between images indicates greater speed.

2) Finite State Machine Implementation: For the terrain-specific gaits, we implemented a finite state machine (FSM) as shown in Fig. 16. For each state, SAIL-R runs with parameters as in Table VIII, selected by the analysis of body speed and COT in Section IV-C. The robot starts in a sampling state with a slow walk to identify the terrain. The cumulative probability from each stride can trigger a transition of states and then the robot updates the gait. One special case is the transition from D to hard surfaces; the trot gait of D can cause structural failures of the legs if the surface is not soft. Thus, the controller detects the normal force beyond a threshold level to identify such a transition, which can proceed immediately.

3) Performance Evaluation: We evaluated the real-time classification and adaptive running by comparing it with a steady fast walk gait. For both test cases, we conducted 9 test runs on a track transitioning from HF ($\mu_k = 1$) to D. We measured average body speeds and COTs on the track of 1 m length (50 cm for each terrain).

The real-time classification result (Fig. 17) shows that the proposed CP algorithm improves classification on hard surfaces and detects the transition within 2-3 strides.

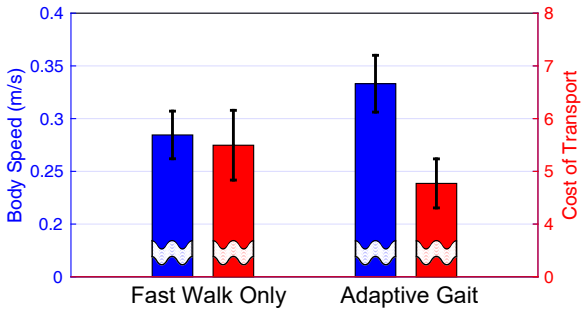

Fig. 19: Robot performance comparison between fast walk (RPM: 300) and an adaptive gait in transition from HF to D.

Using the proposed FSM, SAIL-R adapts its gait, achieving faster and more efficient running. Figure 18 shows high speed video overlays, comparing a steady fast walk gait and an adaptive gait. SAIL-R was able to change its gait to faster trot gaits on D. Figure 19 shows robot speed and COT for adaptive and non-adaptive gaits; we measured 9 trials for each case. As expected from gait evaluations (Fig. 7 and Fig. 8) SAIL-R achieves better running performance with an adaptive gait: on average, 17.1% faster speeds and 13.2% lower COT.

G. Conclusions

We have presented an approach for using tactile sensors on the feet of a small robot to identify terrains and adapt its gait in response to terrain changes. The sensors are capacitive, fabricated using flexible printed circuit technology, with local processing to reduce wiring to the rotary legs.

The sensors consist of five normal force taxels and one shear sensor, sampled at 217 Hz. The resulting information is sufficient to characterize interactions between the legs and the ground. Key features from the tactile data include impact forces, contact duration, and leg contact locations. Using tactile sensing information combined with motor measurements, we constructed a SVM classifier which distinguishes between the four terrain classes with 82.5% overall accuracy. The main source of error is between otherwise similar hard surfaces with moderate ($\mu = 0.5$) or high ($\mu = 1$) friction.

For gait selection, we tested two different gaits (fast-walk and trot) on four types of terrain. In terms of stability, speeds and cost of transport, fast-walk gaits perform better on hard and granular surfaces, while a trod gait performed better on deformable surfaces.

Using a simplified version of the terrain classifier for real-time computation, we implemented a gait adaptation system. To compensate for a lower classification accuracy we implemented a cumulative probability classifier. The resulting gait adaptation detects the transition between two terrains within two strides and demonstrates 17.1% increase in body speed and 13.2% decrease in COT as compared to an unchanging fast-walk gait.

As future work, the optimized gait parameters for each terrain type can be suggested from thorough parametric studies, similar to [78]. If more powerful onboard computation is available, the terrain based control could also employ a

classifier with higher accuracy and detect transitions more rapidly; potential candidates are deep learning algorithms, such as RNN and LSTM. The proposed tactile sensory system can also be useful for walking on rough terrain in planning leg placements for stable walking.

V. Acknowledgments

The work in this paper was supported in part by the Army Research Laboratory under the MAST Collaborative Technology Alliance (MAST-13-2.6). X. A. Wu was supported by the National Science Foundation Graduate Research Fellowship, T. M. Huh was supported by a Samsung Scholarship. A. Sabin was supported by the Stanford ME REU program. S. A. Suresh was supported by a NASA Space Technology Research Fellowship (NSTRF).

References

[1] C. Li, P. B. Umbanhowar, H. Komsuoglu, D. E. Koditschek, and D. I. Goldman, "Sensitive dependence of the motion of a legged robot on granular media," *Proceedings of the National Academy of Sciences*, vol. 106, no. 9, pp. 3029–3034, 2009.

[2] A. Pullinz, R. S. Fearing, and D. I. Goldman, "Walking and running on yielding and fluidizing ground," *Robotics: Science and Systems*, 2012.

[3] F. Delcomyn, M. E. Nelson, and J. H. Cocatre-Zilgien, "Sense organs of insect legs and the selection of sensors for agile walking robots," *IJRR*, vol. 15, no. 2, pp. 113–127, 1996.

[4] M. Maggiali, G. Cannata, P. Maiolino, G. Metta, M. Randazzo, and G. Sandini, "Embedded distributed capacitive tactile sensor," in *Mechatronics Forum Biennial International Conference 2008, University of Limerick, Ireland,*, June 2008.

[5] B. Heyneman and M. R. Cutkosky, "Slip classification for dynamic tactile array sensors," *IJRR*, p. 0278364914564703, 2015.

[6] U. Kim, D.-H. Lee, H. Moon, J. C. Koo, and H. R. Choi, "Design and realization of grasper-integrated force sensor for minimally invasive robotic surgery," in *IEEE/RSJ IROS*. IEEE, 2014, pp. 4321–4326.

[7] A. Naidu, R. Patel, and M. Naish, "Low-cost disposable tactile sensors for palpation in minimally invasive surgery," *IEEE/ASME Transactions on Mechatronics*, pp. 127–137, 2016.

[8] J. Raibert MH, Brown HB, "Experiments in balance with a 2d one-legged hopping machine," *Journal of Dynamic Systems, Measurement, and Control*, vol. 106, no. 1, pp. 75–81, 1984.

[9] M. H. Raibert, H. B. Brown, and M. Chepponis, "Experiments in balance with a 3d one-legged hopping machine," *The International Journal of Robotics Research*, vol. 3, no. 2, pp. 75–92, 1984.

[10] S. Hirose, "A study of design and control of a quadruped walking vehicle," *The International Journal of Robotics Research*, vol. 3, no. 2, pp. 113–133, 1984.

[11] K. Waldron and R. McGhee, "The adaptive suspension vehicle," *IEEE Control Systems Magazine*, vol. 6, no. 6, pp. 7–12, 1986.

[12] K. Hirai, M. Hirose, Y. Haikawa, and T. Takenaka, "The development of honda humanoid robot," in *Robotics and Automation, 1998. Proceedings. 1998 IEEE International Conference on*, vol. 2. IEEE, 1998, pp. 1321–1326.

[13] N. G. Tsagarakis, G. Metta, G. Sandini, D. Vernon, R. Beira, F. Becchi, L. Righetti, J. Santos-Victor, A. J. Ijspeert, M. C. Carrozza, *et al.*, "icub: the design and realization of an open humanoid platform for cognitive and neuroscience research," *Advanced Robotics*, vol. 21, no. 10, pp. 1151–1175, 2007.

[14] M. Zucker, S. Joo, M. X. Grey, C. Rasmussen, E. Huang, M. Stilman, and A. Bobick, "A general-purpose system for teleoperation of the drc-hubo humanoid robot," *Journal of Field Robotics*, vol. 32, no. 3, pp. 336–351, 2015.

[15] G. M. Atmeh, I. Ranatunga, D. O. Popa, K. Subbarao, F. Lewis, and P. Rowe, "Implementation of an adaptive, model free, learning controller on the atlas robot," in *American Control Conference (ACC), 2014*. IEEE, 2014, pp. 2887–2892.

[16] K. Nishiwaki, J. Kuffner, S. Kagami, M. Inaba, and H. Inoue, "The experimental humanoid robot h7: a research platform for autonomous behaviour," *Philosophical Transactions of the Royal Society of London A: Mathematical, Physical and Engineering Sciences*, vol. 365, no. 1850, pp. 79–107, 2007.

[17] M. Y. Chuah and S. Kim, "Enabling force sensing during ground locomotion: A bio-inspired, multi-axis, composite force sensor using discrete pressure mapping," *IEEE Sensors Journal*, vol. 14, no. 5, pp. 1693–1703, 2014.

[18] D. Kuehn, F. Grimminger, F. Beinersdorf, F. Bernhard, A. Burchardt, M. Schilling, M. Simnofske, T. Stark, M. Zenzes, and F. Kirchner, "Additional dofs and sensors for bio-inspired locomotion: Towards active spine, ankle joints, and feet for a quadruped robot," in *Robotics and Biomimetics (ROBIO), 2011 IEEE International Conference on*. IEEE, 2011, pp. 2780–2786.

[19] J. K. Karpick, J. G. Cham, J. E. Clark, and M. R. Cutkosky, "Stride period adaptation for a biomimetic running hexapod," in *Robotics Research*. Springer, 2003, pp. 133–145.

[20] D. W. Haldane, C. S. Casarez, J. T. Karras, J. Lee, C. Li, A. O. Pullin, E. W. Schaler, D. Yun, H. Ota, A. Javey, *et al.*, "Integrated manufacture of exoskeletons and sensing structures for folded millirobots," *Journal of Mechanisms and Robotics*, vol. 7, no. 2, p. 021011, 2015.

[21] J. D. Goldberg and R. S. Fearing, "Force sensing shell using a planar sensor for miniature legged robots," in *Intelligent Robots and Systems (IROS), 2015 IEEE/RSJ International Conference on*. IEEE, 2015, pp. 1494–1500.

[22] H. Yousef, M. Boukallel, and K. Althoefer, "Tactile sensing for dexterous in-hand manipulation in robotics—a review," *Sensors and Actuators A: physical*, vol. 167, no. 2, pp. 171–187, 2011.

[23] R. S. Dahiya, G. Metta, M. Valle, and G. Sandini, "Tactile sensing—from humans to humanoids," *Robotics, IEEE Transactions on*, vol. 26, no. 1, pp. 1–20, 2010.

[24] M. R. Cutkosky and J. Ulmen, "Dynamic tactile sensing," in *The Human Hand as an Inspiration for Robot Hand Development*. Springer, 2014, pp. 389–403.

[25] M. R. Cutkosky and W. Provancher, *Force and Tactile Sensing*. Springer International Publishing, 2016, pp. 717–736.

[26] K. C. Galloway, J. E. Clark, and D. E. Koditschek, "Variable stiffness legs for robust, efficient, and stable dynamic running," *Journal of Mechanisms and Robotics*, vol. 5, no. 1, p. 011009, 2013.

[27] A. S. Boxerbaum, J. Oro, G. Peterson, and R. D. Quinn, "The latest generation whegs™ robot features a passive-compliant body joint," in *Intelligent Robots and Systems, 2008. IROS 2008. IEEE/RSJ International Conference on*. IEEE, 2008, pp. 1636–1641.

[28] A. Shashank, M. Tiwana, S. Redmond, and N. Lovell, "Design, simulation and fabrication of a low cost capacitive tactile shear sensor for a robotic hand," in *IEEE EMBC*. IEEE, 2009, pp. 4132–4135.

[29] J. Ulmen and M. Cutkosky, "A robust, low-cost and low-noise artificial skin for human-friendly robots," in *IEEE ICRA*. IEEE, 2010, pp. 4836–41.

[30] A. Schmitz, P. Maiolino, M. Maggiali, L. Natale, G. Cannata, and G. Metta, "Methods and technologies for the implementation of large-scale robot tactile sensors," *Robotics, IEEE Transactions on*, vol. 27, no. 3, pp. 389–400, 2011.

[31] D. M. Aukes, B. Heyneman, J. Ulmen, H. Stuart, M. R. Cutkosky, S. Kim, P. Garcia, and A. Edsinger, "Design and testing of a selectively compliant underactuated hand," *IJRR*, p. 0278364913518997, 2014.

[32] X. A. Wu, T. M. Huh, R. Mukherjee, and M. Cutkosky, "Integrated ground reaction force sensing and terrain classification for small legged robots," *IEEE Robotics and Automation Letters*, vol. 1, no. 2, pp. 1125–1132, 2016.

[33] T. A. McMahon and P. R. Greene, "The influence of track compliance on running," *Journal of biomechanics*, vol. 12, no. 12, pp. 893–904, 1979.

[34] D. P. Ferris, M. Louie, and C. T. Farley, "Running in the real world: adjusting leg stiffness for different surfaces," *Proceedings of the Royal Society of London B: Biological Sciences*, vol. 265, no. 1400, pp. 989–994, 1998.

[35] S. Rossignol, J. Lund, and T. Drew, "The role of sensory inputs in regulating patterns of rhythmical movements in higher vertebrates," *Neural control of rhythmic movements in vertebrates*, pp. 201–283, 1988.

[36] J. C. Spagna, D. I. Goldman, P.-C. Lin, D. E. Koditschek, and R. J. Full, "Distributed mechanical feedback in arthropods and robots simplifies control of rapid running on challenging terrain," *Bioinspiration & biomimetics*, vol. 2, no. 1, p. 9, 2007.

[37] A. J. Spence, S. Revzen, J. Seipel, C. Mullens, and R. J. Full, "Insects running on elastic surfaces," *Journal of Experimental Biology*, vol. 213, no. 11, pp. 1907–1920, 2010.

[38] J. G. Cham, J. K. Karpick, and M. R. Cutkosky, "Stride period adaptation of a biomimetic running hexapod," *The International Journal of Robotics Research*, vol. 23, no. 2, pp. 141–153, 2004.

[39] C. Li, T. Zhang, and D. I. Goldman, "A terradynamics of legged locomotion on granular media," *Science*, vol. 339, no. 6126, pp. 1408–1412, 2013.
[40] V. R. Kumar and K. J. Waldron, "Adaptive gait control for a walking robot," *Journal of Field Robotics*, vol. 6, no. 1, pp. 49–76, 1989.
[41] Y. Fukuoka, H. Kimura, and A. H. Cohen, "Adaptive dynamic walking of a quadruped robot on irregular terrain based on biological concepts," *The International Journal of Robotics Research*, vol. 22, no. 3-4, pp. 187–202, 2003.
[42] H. Kimura, Y. Fukuoka, and A. H. Cohen, "Adaptive dynamic walking of a quadruped robot on natural ground based on biological concepts," *The International Journal of Robotics Research*, vol. 26, no. 5, pp. 475–490, 2007.
[43] Z. G. Zhang, Y. Fukuoka, and H. Kimura, "Adaptive running of a quadruped robot using delayed feedback control," in *Robotics and Automation, 2005. ICRA 2005. Proceedings of the 2005 IEEE International Conference on*. IEEE, 2005, pp. 3739–3744.
[44] J. D. Weingarten, G. A. Lopes, M. Buehler, R. E. Groff, and D. E. Koditschek, "Automated gait adaptation for legged robots," in *Robotics and Automation, 2004. Proceedings. ICRA'04. 2004 IEEE International Conference on*, vol. 3. IEEE, 2004, pp. 2153–2158.
[45] G. C. Haynes and A. A. Rizzi, "Gaits and gait transitions for legged robots," in *Robotics and Automation, 2006. ICRA 2006. Proceedings 2006 IEEE International Conference on*. IEEE, 2006, pp. 1117–1122.
[46] C. Brooks, K. Iagnemma, *et al.*, "Vibration-based terrain classification for planetary exploration rovers," *IEEE Trans. on Robotics*, vol. 21, no. 6, pp. 1185–1191, 2005.
[47] C. Weiss, H. Frohlich, and A. Zell, "Vibration-based terrain classification using support vector machines," in *IEEE/RSJ IROS*. IEEE, 2006, pp. 4429–4434.
[48] K. Iagnemma and S. Dubowsky, "Terrain estimation for high-speed rough-terrain autonomous vehicle navigation," in *Proceedings of the SPIE Conference on Unmanned Ground Vehicle Technology IV*, vol. 4715, 2002, p. 1.
[49] L. Ojeda, J. Borenstein, G. Witus, and R. Karlsen, "Terrain characterization and classification with a mobile robot," *Journal of Field Robotics*, vol. 23, no. 2, pp. 103–122, 2006.
[50] C. A. Brooks and K. Iagnemma, "Self-supervised terrain classification for planetary surface exploration rovers," *Journal of Field Robotics*, vol. 29, no. 3, pp. 445–468, 2012.
[51] E. M. Dupont, C. A. Moore, E. G. Collins, and E. Coyle, "Frequency response method for terrain classification in autonomous ground vehicles," *Autonomous Robots*, vol. 24, no. 4, pp. 337–347, 2008.
[52] E. M. DuPont, E. Collins, E. J. Coyle, and R. G. Roberts, "Terrain classification using vibration sensors: theory and methods," *New Research on Mobile Robotics*, 2008.
[53] A. Angelova, L. Matthies, D. Helmick, and P. Perona, "Fast terrain classification using variable-length representation for autonomous navigation," in *Computer Vision and Pattern Recognition, 2007. CVPR'07. IEEE Conference on*. IEEE, 2007, pp. 1–8.
[54] P. Filitchkin and K. Byl, "Feature-based terrain classification for littledog," in *IEEE/RSJ IROS*. IEEE, 2012, pp. 1387–1392.
[55] K. Walas and M. Nowicki, "Terrain classification using laser range finder," in *IEEE/RSJ IROS*. IEEE, 2014, pp. 5003–5009.
[56] S. Zenker, E. E. Aksoy, D. Goldschmidt, F. Worgotter, and P. Manoonpong, "Visual terrain classification for selecting energy efficient gaits of a hexapod robot," in *Advanced Intelligent Mechatronics (AIM), 2013 IEEE/ASME International Conference on*. IEEE, 2013, pp. 577–584.
[57] D. W. Haldane, P. Fankhauser, R. Siegwart, and R. S. Fearing, "Detection of slippery terrain with a heterogeneous team of legged robots," in *ICRA*. IEEE, 2014, pp. 4576–4581.
[58] J. Libby and A. J. Stentz, "Using sound to classify vehicle-terrain interactions in outdoor environments," in *Robotics and Automation (ICRA), 2012 IEEE International Conference on*. IEEE, 2012, pp. 3559–3566.
[59] P. Giguere and G. Dudek, "A simple tactile probe for surface identification by mobile robots," *IEEE Trans. on Robotics*, vol. 27, no. 3, pp. 534–544, 2011.
[60] K. Walas, "Terrain classification using vision, depth and tactile perception," *Proceedings of the 2013 RGB-D: Advanced Reasoning with Depth Cameras in Conjunction with RSS, Berlin, Germany*, vol. 27, 2013.
[61] A. Schmidt and K. Walas, "The classification of the terrain by a hexapod robot," in *Proceedings of the 8th International Conference on Computer Recognition Systems CORES 2013*. Springer, 2013, pp. 825–833.
[62] M. Höpflinger, C. D. Remy, M. Hutter, L. Spinello, R. Siegwart, *et al.*, "Haptic terrain classification for legged robots," in *ICRA*. IEEE, 2010, pp. 2828–2833.
[63] L. Ascari, M. Ziegenmeyer, P. Corradi, B. Gaßmann, M. Zöllner, R. Dillmann, and P. Dario, "Can statistics help walking robots in assessing terrain roughness? platform description and preliminary considerations," in *Prooceedings of the 9th ESA Workshop on Advanced Space Technologies for Robotics and Automation ASTRA2006, ESTEC, Noordwijk, The Netherlands*, 2006.
[64] J. J. Shill, E. G. Collins Jr, E. Coyle, and J. Clark, "Tactile surface classification for limbed robots using a pressure sensitive robot skin," *Bioinspiration & biomimetics*, vol. 10, no. 1, p. 016012, 2015.
[65] W. Bosworth, J. Whitney, S. Kim, and N. Hogan, "Robot locomotion on hard and soft ground: Measuring stability and ground properties in-situ," in *Robotics and Automation (ICRA), 2016 IEEE International Conference on*. IEEE, 2016, pp. 3582–3589.
[66] F. L. Garcia Bermudez, R. C. Julian, D. W. Haldane, P. Abbeel, and R. S. Fearing, "Performance analysis and terrain classification for a legged robot over rough terrain," in *IEEE/RSJ IROS*. IEEE, 2012, pp. 513–519.
[67] C. Ordonez, J. Shill, A. Johnson, J. Clark, and E. Collins, "Terrain identification for rhex-type robots," in *SPIE Defense, Security, and Sensing*. International Society for Optics and Photonics, 2013, pp. 87 410Q–87 410Q.
[68] P. Giguere and G. Dudek, "Clustering sensor data for autonomous terrain identification using time-dependency," *Autonomous Robots*, vol. 26, no. 2-3, pp. 171–186, 2009.
[69] S. Manjanna, G. Dudek, and P. Giguere, "Using gait change for terrain sensing by robots," in *Computer and Robot Vision (CRV), 2013 International Conference on*. IEEE, 2013, pp. 16–22.
[70] S. Manjanna and G. Dudek, "Autonomous gait selection for energy efficient walking," in *Robotics and Automation (ICRA), 2015 IEEE International Conference on*. IEEE, 2015, pp. 5155–5162.
[71] A. M. Hoover, S. Burden, X.-Y. Fu, S. S. Sastry, and R. S. Fearing, "Bio-inspired design and dynamic maneuverability of a minimally actuated six-legged robot," in *Biomedical Robotics and Biomechatronics (BioRob), 2010 3rd IEEE RAS and EMBS International Conference on*. IEEE, 2010, pp. 869–876.
[72] P. Holmes, R. J. Full, D. Koditschek, and J. Guckenheimer, "The dynamics of legged locomotion: Models, analyses, and challenges," *Siam Review*, vol. 48, no. 2, pp. 207–304, 2006.
[73] A. J. Ijspeert, "Central pattern generators for locomotion control in animals and robots: a review," *Neural Networks*, vol. 21, no. 4, pp. 642–653, 2008.
[74] U. Saranli, M. Buehler, and D. E. Koditschek, "Design, modeling and preliminary control of a compliant hexapod robot," in *Robotics and Automation, 2000. Proceedings. ICRA'00. IEEE International Conference on*, vol. 3. IEEE, 2000, pp. 2589–2596.
[75] R. Blickhan, "The spring-mass model for running and hopping," *Journal of biomechanics*, vol. 22, no. 11-12, pp. 1217–1227, 1989.
[76] M. Hall, E. Frank, G. Holmes, B. Pfahringer, P. Reutemann, and I. H. Witten, "The weka data mining software: an update," *ACM SIGKDD explorations newsletter*, vol. 11, no. 1, pp. 10–18, 2009.
[77] X. A. Wu, N. Burkhard, B. Heyneman, R. Valen, and M. Cutkosky, "Contact event detection for robotic oil drilling," in *Robotics and Automation (ICRA), 2014 IEEE International Conference on*. IEEE, 2014, pp. 2255–2261.
[78] C. Li, P. B. Umbanhowar, H. Komsuoglu, and D. I. Goldman, "The effect of limb kinematics on the speed of a legged robot on granular media," *Experimental mechanics*, vol. 50, no. 9, pp. 1383–1393, 2010.

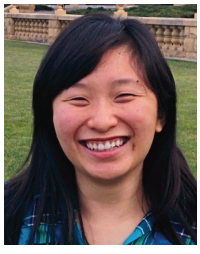

X. Alice Wu (M.S.'13, Ph.D.'17) received the B.S. degree in Biomedical Engineering from Johns Hopkins University in 2011 and the Ph.D. degree in in Mechanical Engineering from Stanford University in 2017. Her research interest is in the area of tactile sensor design and machine learning algorithms for contact event detection in dexterous manipulation and robot locomotion.

Tae Myung Huh (SM'18) received the B.S. degree in mechanical engineering in 2014 from Seoul National University, Seoul, South Korea and the M.S. degree in mechanical engineering in 2016 from Stanford University, Stanford, CA, where he is currently working toward the Ph.D. in mechanical engineering. His research interests include tactile / force-torque sensors, bioinspired robots, sensor networks and perception of grasping.

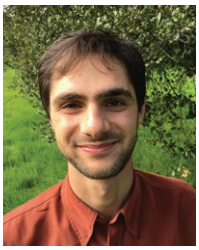

Aaron Sabin earned his B.S. degree from Stanford University in 2017. After graduating, Aaron worked with the Los Angeles Dodgers on their baseball data analytics team, and is now designing golf clubs at Taylormade Golf Co.

Srinivasan A. Suresh (S'17) received the B.S.E. degree in mechanical and aerospace engineering from Princeton Univeristy, Princeton, NJ, USA in 2013. He is currently working toward the Ph.D degree in mechanical engineering at Stanford University under the supervision of Prof. M. Cutkosky. His research interests include the design, testing, and manufacturing of bioinspired dry adhesive structures, along with research and development of robotic systems leveraging these adhesives for improved capabilities and performance, particularly for microgravity applications. Mr. Suresh was the recipient of one IROS Best Paper award as a coauthor.

Mark R. Cutkosky (F'12) received the Ph.D. degree in mechanical engineering from Carnegie Mellon University, Pittsburgh, PA, USA, in 1985. He is the Fletcher Jones Professor in mechanical engineering at Stanford University, Stanford, CA, USA. His research interests include bioinspired robots, haptics and rapid prototyping processes. Dr. Cutkosky is a Fellow of the ASME and IEEE.